9-29-2005

Structure of Human Thymidylate Synthase under Low-Salt Conditions

Leslie L. Lovelace
University of South Carolina - Columbia, lovelacl@mailbox.sc.edu

Wladek Minor
University of Virginia

Lukasz Lebioda
University of South Carolina - Columbia, lebioda@mailbox.sc.edu

Publication Info

Published in *Acta Crystallographica Section D: Biological Crystallography*, Volume 61, Issue 5, 2005, pages 622-627.

Acta Crystallographica Section D
Biological Crystallography
ISSN 0907-4449

Structure of human thymidylate synthase under low-salt conditions

Leslie L. Lovelace,[a] Wladek Minor[b] and Lukasz Lebioda[a,c]*

[a]Department of Chemistry and Biochemistry, University of South Carolina, Columbia, SC 29208, USA, [b]Department of Biophysics and Molecular Pharmacology, University of Virginia, Charlottesville, VI 48824, USA, and [c]Center for Colon Cancer Research, University of South Carolina, Columbia, SC 29208, USA

Correspondence e-mail: lebioda@mail.chem.sc.edu

Received 29 September 2004
Accepted 23 February 2005

PDB Reference: thymidylate synthase, 1ypv, r1ypvsf.

Human thymidylate synthase, a target in cancer chemotherapy, was crystallized from PEG 3350 with 30 m*M* ammonium sulfate (AS) in the crystallization medium. The crystals are isomorphous with the high-salt crystals (~2.0 *M* AS) and the structure has been solved and refined ($R = 22.6\%$, $R_{\rm free} = 24.3\%$) at 1.8 Å resolution. The high- and low-AS-concentration structures are quite similar, with loop 181–197 is in the inactive conformation. Also, residues 95–106 and 129–135 (eukaryotic inserts region) show high mobility as assessed by poor electron density and high values of crystallographic temperature factors (residues 1–25 and 108–129 are disordered in both structures). The high mobility of this region may reflect the situation at physiological ionic strength. Of the four sulfate ions observed bound at 2.0 *M* AS, only two are present at 30 m*M* AS. The inactive conformation appears to be stabilized by the side chain of Val3 or a leucine residue from the disordered regions. The low-salt conditions of these crystals should be much more suitable for the study of thymidylate synthase inhibitors, especially those that utilize sulfate-binding sites to stabilize the inactive conformation of loop 181–197.

1. Introduction

Thymidylate synthase (TS) catalyzes the reaction in which the nucleotide deoxyuridylate (dUMP) is reductively methylated by the folate co-substrate 5,10-methylenetetrahydrofolate (CH_2H_4PteGlu) to form thymidylate (TMP) and dihydrofolate (Humphries & Greenberg, 1958). The enzyme is a dimer of two identical subunits, which generate an asymmetry upon substrate/ligand binding (Danenberg & Danenberg, 1979; Anderson *et al.*, 1999). Substrates are bound in an ordered manner, with dUMP binding at the active site prior to CH_2H_4PteGlu. A cysteine residue (Cys195 in human TS; hTS) at the active site attacks the 6-position of the pyrimidine base of the nucleotide, resulting in the formation of a covalent bond between TS and the nucleotide and activating the 5-position of the nucleotide for subsequent covalent-bond formation with the C-11 substituent of CH_2H_4PteGlu (reviewed by Carreras & Santi, 1995; Stroud & Finer-Moore, 2003; Finer-Moore *et al.*, 2003).

The enzyme is the sole source of *de novo* synthesized thymidylate and its inhibition leads to apoptosis of rapidly dividing cells such as cancer cells, an effect sometimes referred to as thymineless death (Houghton, 1999). This phenomenon is exploited in therapeutic protocols utilizing TS inhibitors, such as raltitrexed, pemetrexed or pro-drugs such as 5-fluorouracil that are metabolized to TS inhibitors. The inhibitors are either nucleotide analogs such as 5-fluorodeoxyuridylate (FdUMP) or folate analogues and are collectively referred to

as antifolates. The effectivness of TS-directed chemotherapy is often limited by emerging resistance, which usually arises from an increase in intracellular TS protein levels by a factor of 2–4 (reviewed in Forsthoefel *et al.*, 2004). Two major mechanisms leading to increased hTS levels have been proposed. In one mechanism, the intracellular turnover of hTS protein is decreased upon formation of inhibitory complexes with drugs (Kitchens *et al.*, 1999; Forsthoefel *et al.*, 2004). The other mechanism is related to hTS protein binding to its own mRNA and inhibiting its translation. The formation of inhibitory complexes competes with mRNA binding and thus reduces the translational repression of hTS (reviewed in Chu & Allegra, 1996).

Human TS differs from bacterial TS in three regions: the N-terminus of hTS is extended by 28–29 residues and two insertions of 12 and eight residues are present at positions 117 and 146, respectively, in the human protein (Carreras & Santi, 1995). The crystal structure of hTS has been determined using crystals obtained at high ammonium sulfate (AS) concentrations (Schiffer *et al.*, 1995; Phan, Steadman *et al.*, 2001). It showed that active-site loop 181–197 is in a conformation different from that observed in bacterial TS. Since this conformation places Cys195, a residue crucial for catalytic activity, outside the active site, the conformer must be inactive. Another characteristic feature was that loop 108–129, which contains one of the eukaryotic inserts, was disordered. There were four sulfate ions bound per subunit. Studies of a truncated version of hTS (Almog *et al.*, 2001) and an inhibitory complex of hTS with dUMP and raltitrexed (Phan, Koli *et al.*, 2001) yielded high-resolution structures of hTS with loop 181–197 in the active conformation. In these structures, determined at low salt concentration, loop 108–129 was ordered. A superposition of the active and inactive conformers is shown in Fig. 1. Intrinsic fluorescence studies of hTS showed that in solution there is an equilibrium between the active and inactive conformers and that the presence of phosphate or sulfate ions drives the equilibrium towards the inactive conformation, while dUMP, a substrate, drives it towards the active conformation (Phan, Steadman *et al.*, 2001). It was proposed that the stabilization of the inactive conformation as a means to achieve hTS inhibition may yield therapeutic outcomes superior to those of classical active-site-directed inhibitors as it may not lead to increased levels of TS (Phan, Steadman *et al.*, 2001; Berger *et al.*, 2004). To facilitate structure-based design of inhibitors that lock hTS in the inactive conformation we have crystallized hTS at a low AS concentration that should allow binding of anionic ligands in crystal soaking experiments. The low-salt hTS structure is reported here at 1.8 Å resolution.

Table 1
Crystallographic data and refinement statistics for hTS.

Values in parentheses are for the outermost resolution shell.

X-ray source	APS SBC-CAT ID
Detector	3 × 3 mosaic
Wavelength (Å)	0.91963
Temperature (K)	100
No. of frames (high/low-resolution passes)	126/63
Oscillation range (high/low-resolution passes) (°)	0.5/1.0
Crystal-to-detector distance (high/low-resolution passes) (mm)	180/220
Space group	$P3_121$
Unit-cell parameters	
a (Å)	95.77
c (Å)	81.81
Volume (Å^3)	650175
Mosaicity (°)	0.49
Resolution range (Å)	50.0–1.8 (1.86–1.80)
Average *I*	23114 (708)
Total No. of reflections	181168
No. of unique reflections	37932 (3639)
Completeness (%)	93.6 (91.2)
Linear R_{merge} in 50.00–3.88 Å shell	0.042
Total linear R_{merge}† (with 0% rejections)	0.060 (0.563)
Square R_{merge}	0.053 (0.487)
No. of reflections in refinement with ($\|F\|/\sigma\|F\| > 0$)	35328 [87.2%]
R value‡	0.226
R_{free}§ (%)	0.243
R.m.s.d. bond lengths (Å)	0.006
R.m.s.d. bond angles (°)	1.4
Ramachandran statistics, residues in	
Most favored region (%)	89.2
Additionally allowed region (%)	10.8
Ligands	2 sulfate ions
No. of water molecules	138

† $R_{merge} = 100\sum|I(h) - \langle I(h)\rangle|/\sum I(h)$, where $I(h)$ is the observed intensity and $\langle I(h)\rangle$ is the mean intensity of reflection h over all measurements of $I(h)$. ‡ *R* factor = $100\sum|F_o - F_c|/\sum F_o$, the sums being taken over all reflections with $F/\sigma(F) > 2$ cutoff. § R_{free} = *R* factor for data that were not included in crystallographic refinement. 4.4% of the reflections were used for calculation of R_{free}.

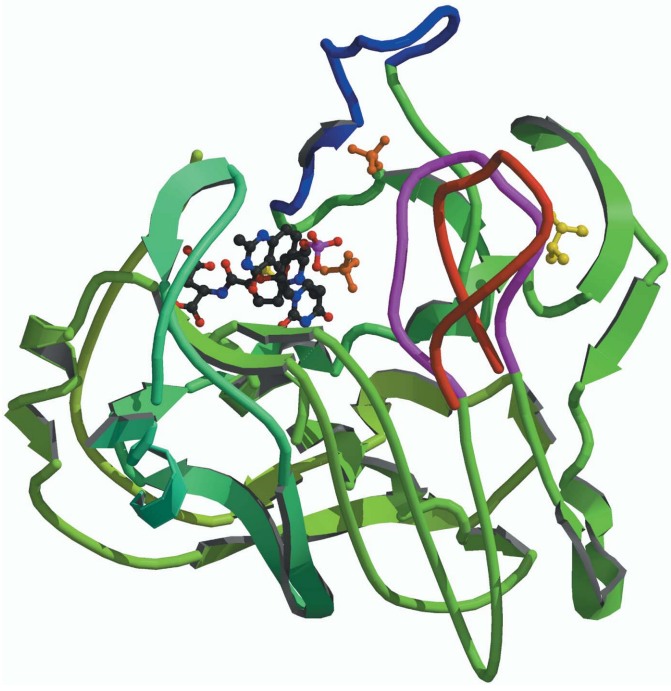

Figure 1
Folding of the active and inactive conformer of hTS. Only one subunit of the dimer is shown. The constant region is shown in green. Loop 181–197 in the active conformer is shown in purple and in the inactive conformer in red. Loop 108–129 in the active conformer is shown in blue; this loop is disordered in the inactive conformer. The location of the active site is indicated by the positions of dUMP and a folate (raltitrexed). The sulfate ions present in the inactive conformer are shown in orange and the valine stabilizing the inactive conformer (perhaps Val3) in yellow.

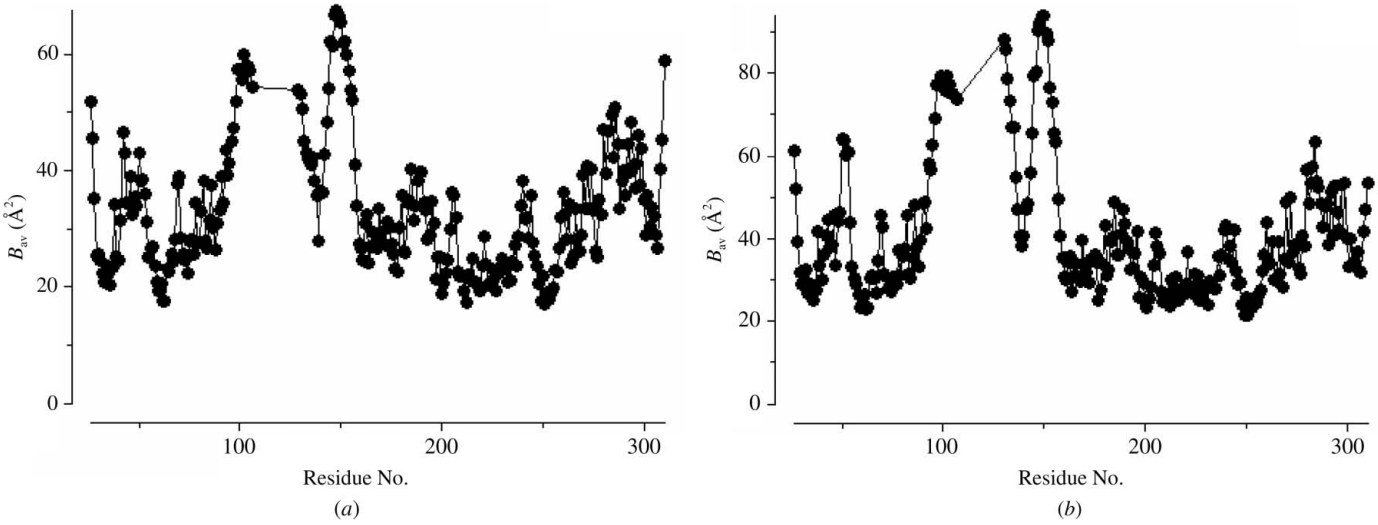

Figure 2
Comparison of the *B* factors for low-AS and high-AS structures of hTS plotted using the *CCP*4 program suite (Collaborative Computational Project, Number 4, 1994). The average *B* factor in the high-AS structure is lower by 7.1 Å^2.

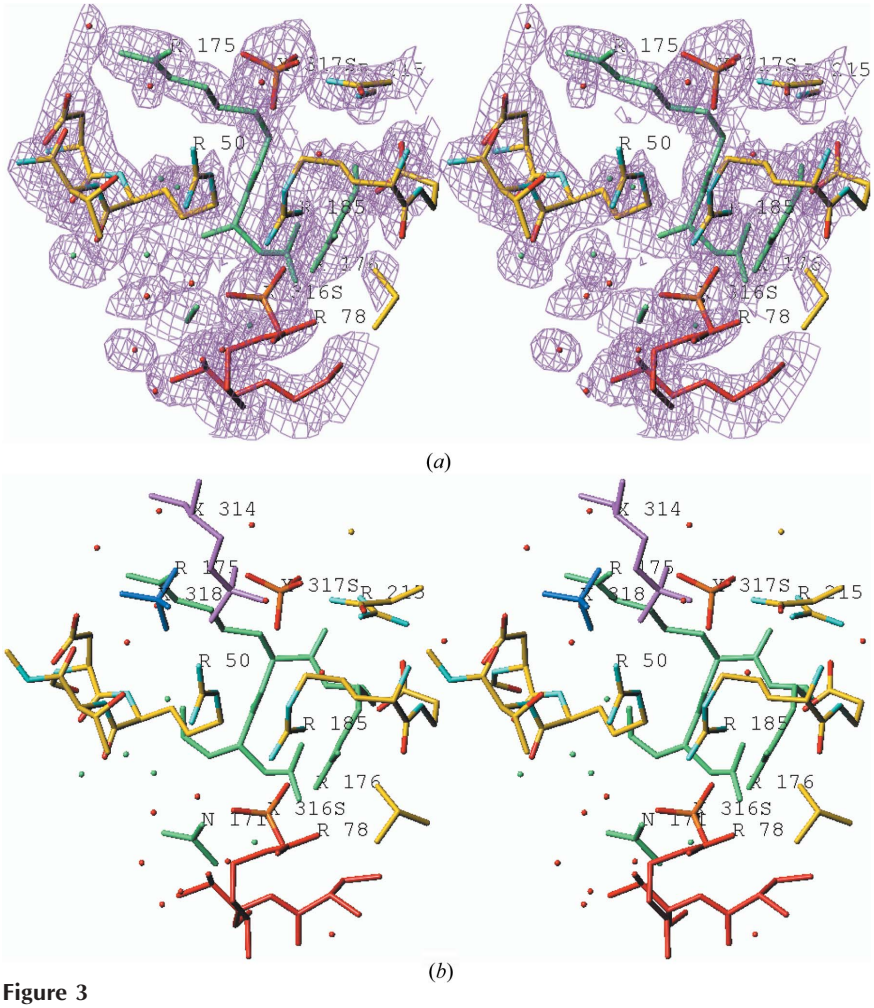

Figure 3
Sulfate-binding region of hTS, located at the junction of three subunits. The subunits in yellow and green form the physiological dimer; the subunit in red is from crystal contacts. (*a*) Electron density in the final $2F_o - F_c$ map contoured at the 1σ level. (*b*) The position of the additional sulfate ion present in the 2.0 *M* AS structure is shown in blue. A fragment of dUMP bound in the active conformer is shown in purple (Phan, Koli *et al.*, 2001); its phosphate position does not correspond to any of the sulfate-binding sites in the inactive conformer.

2. Experimental

2.1. Protein expression and crystallization

Recombinant hTS was expressed and purified as described previously (Phan, Steadman *et al.*, 2001) with minor modifications. Briefly, the cell-free extract was first chromatographed on a Q-Sepharose anion-exchange column followed by buffer-exchange of the active fractions. The resulting supernatant was then passed through a Blue Sepharose CL-6B column. The active fractions were pooled and analyzed by SDS–PAGE for purity. Crystals of hTS were grown under low-salt conditions (30 m*M* ammonium sulfate, 30–40% PEG 4K, 0.1 *M* Tris pH 8.5, 20 m*M* βME) by sitting-drop vapour diffusion. High-salt crystals were obtained using the same buffer and pH but using 38–50% saturated ammonium sulfate as precipitant and 40 m*M* phosphate (Phan, Steadman *et al.*, 2001).

2.2. Data collection and processing

An hTS crystal was transferred to cryosolvent (mother liquor brought to 10% in ethylene glycol) for a few seconds and flash-frozen. X-ray diffraction data were collected at the SBC-CAT ID beamline at APS, Argonne National Laboratory at a wavelength of 0.97929 Å. Two passes were used: one with 0.5° oscillation range and the other with 1.0° oscillation range. Although 90° of data were collected, the rapid rise in R_{merge} limited the useful data to 126 frames

for the high-resolution scan and 63 frames for the low-resolution scan. The data were indexed and processed with *HKL*2000 (Otwinowski & Minor, 1997); processing parameters and statistics are summarized in Table 1.

2.3. Structure determination and refinement

The structure was solved by molecular replacement using *CNS* (Brünger *et al.*, 1998) with the structure obtained under high-salt conditions (PDB code 1hw3; Phan, Steadman *et al.*, 2001) as the search model. This approach was selected since the unit cells had *c* parameters that differed by 1.4 Å. Crystallographic refinement was carried out with iterative combination of interactive graphics utilizing *TURBO-FRODO* (Roussel & Cambillau, 1991) and simulated annealing using *CNS*. Water molecules were assigned to peaks that were present in both $F_o - F_c$ and $2F_o - F_c$ maps and formed appropriate contacts with the protein molecule. Water molecules that had a *B* factor above 75 Å^2 after refinement were deleted. The correctness of the structure was evaluated using *PROCHECK* (Laskowski *et al.*, 1993).

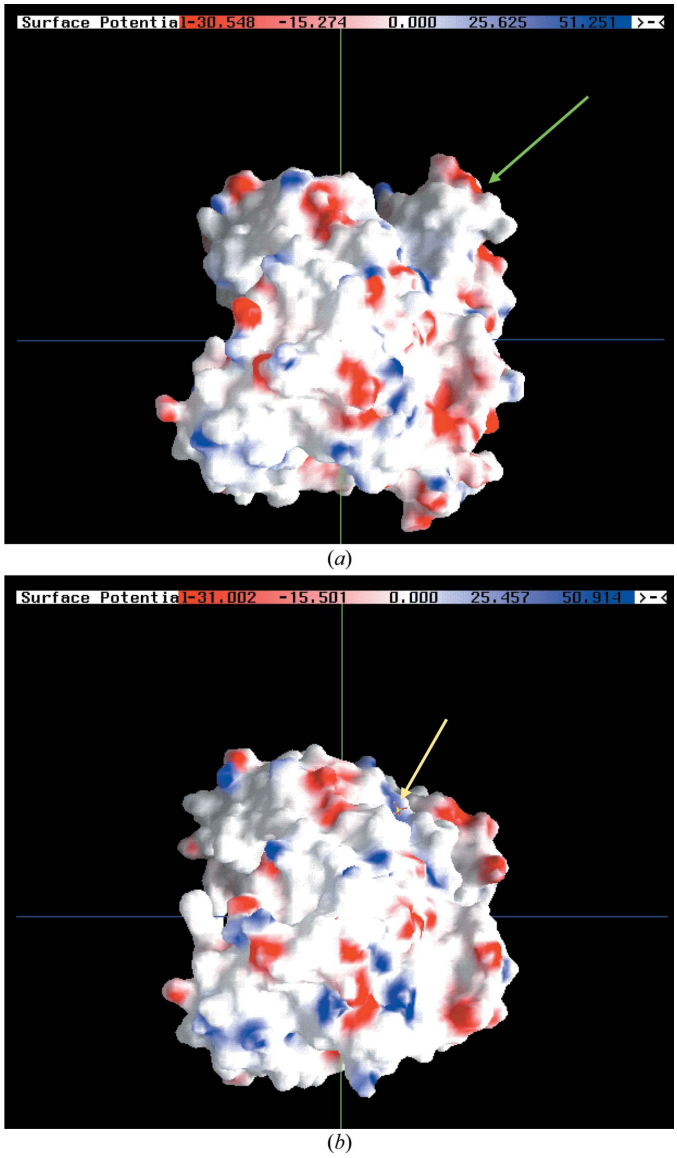

Figure 4
Molecular electrostatic potential of hTS. (*a*) Active conformer (Almog *et al.*, 2001; PDB code 1hzw). The arrow points to the region of ordered loop 108–129. (*b*) Inactive conformer (this report). The arrow points to one of the bound sulfate ions; the other is buried and not visible.

2.4. Superposition and graphics

Superposition of the protein models was carried out using the *LSQKAB* program from the *CCP*4 package (Collaborative Computational Project, Number 4, 1994). Fig. 1 was prepared using *MOLSCRIPT* (Kraulis, 1991) and *RASTER3D* (Merritt & Bacon, 1997), Fig. 2 was prepared with the *BPLOT* program from the *CCP*4 package and Figs. 3 and 5 were generated using *TURBO-FRODO*. Calculations of the molecular electrostatic potential were carried out with *DELPHI* (Rocchia *et al.*, 2001, 2002) and displayed in Fig. 4 with *GRASP* (Nicholls *et al.*, 1991).

3. Results and discussion

Despite large differences in the composition of the mother liquors, the high-salt (2.0 *M* AS) crystals and low-salt (30 m*M* AS) crystals of hTS have the same space group $P3_121$ and similar unit-cell parameters: $a = 95.82$, $c = 83.21$ Å and $a = 95.77$, $c = 81.81$ Å, respectively. This indicates that the principal determinants of crystal packing are similar for both crystallization conditions.

In general, the low-salt crystals of hTS are of similar quality to the high-salt crystals. Although we report data at the somewhat higher resolution of 1.8 Å compared with 2.0 Å, this may reflect progress in beamline instrumentation rather than the crystal quality. The somewhat higher values of the *R* factors (22.6 and 24.3%) are likely to be a result of the disorder of ∼16% of the protein. There are some stretches of electron density that are not interpretable (see below) but which are likely to contribute to X-ray scattering. A superposition of the high- and low-AS structures yielded average and r.m.s. displacements of 0.19 and 0.40 Å, respectively. The largest difference, 5.4 Å, was at Gly52, where a loop was rebuilt; it is more likely to reflect reinterpretation of better electron density than a real structural change. A comparison of the average temperature factors is shown in Fig. 2. The absolute values of temperature factors may to some degree depend on the resolution, crystal mosaicity and other parameters of data processing, but the relative distribution of *B* factors is more reliable. It shows high similarity except for the regions adjacent to the disordered fragments of the molecule, where the *B* factors are somewhat higher for the low-salt conditions. This suggests that under physiological conditions, which are closer to the low-salt crystallization conditions, loop 108–129 is at least as mobile as it is under the high-salt conditions. This confirms that the disorder/mobility of this loop correlates with the inactive conformation of loop 181–197 and not with the ionic strength of the solution. This is an important distinction, since the hTS structures in the active conformation, the truncation mutant (Almog *et al.*, 2001) and

the inhibitory complex (Phan, Koli *et al.*, 2001), which had the loop ordered, were determined at low ionic strength. It was suggested that the mobility of loop 108–129 may facilitate in priming hTS for degradation (Berger *et al.*, 2004); thus, the data presented here are consistent with the hypothesis that the inactive conformer of hTS is more prone to turnover.

Four sulfate ions were bound per subunit in the high-AS-concentration structure. It was speculated that three of them, clustered in the vicinity of the active site, may map the positions of mRNA phosphates (Phan, Steadman *et al.*, 2001). The fourth sulfate ion was located far from the active-site region; it is not present in the low-salt structure. The cluster of three sulfate ions in the vicinity of the active site observed at high AS concentration is reduced to two at low AS. One binding site is conserved; the position of the other is shifted by about 0.8 Å (Fig. 3). This shows the adaptability of the arginine residues that line this part of hTS molecule. It should be indicated that hTS in the active conformation binds only one phosphate ion (at 50 m*M* P_i concentration) in a position that corresponds to the phosphate moiety of the dUMP substrate (Almog *et al.*, 2001). This position is significantly different from the binding sites observed in the inactive conformer (Fig. 3). Thus, the transition from the active to inactive conformation of loop 181–197 affects the distribution of surface charges and anion-binding properties. A comparison of the molecular electrostatic potential of hTS in the active and inactive conformation is shown in Fig. 4.

Other differences between the high-AS and low-AS structures include the lack of bound glycol, a cryosolvent molecule, which is replaced by two water molecules in the low-salt structure. On the other hand, in the low-AS-concentration structure, clear density is present in a hydrophobic pocket formed by residues Phe137, Gln138, Phe142, Gly143, Trp182 and Leu187 (Fig. 5). We modeled a valine residue into it, but leucine is also a possibility. The pocket is only present in the inactive conformer and the density does not correspond to any fragment of loop 181–197 in the active conformation. If it is considered that the Δ6–29 mutant, an hTS variant missing residues 6–29, crystallized with loop 181–197 in the active conformation under very similar crystallization conditions, it appears likely that the Δ6–29 deletion affects loop 181–197. The unconnected valine (or leucine) residue interacts with loop 181–197 and presumably stabilizes the inactive conformer. Its position with respect to the loop is shown in Fig. 1. One interpretation is that this residue is a part of the N-terminus, which is disordered in all reported crystal structures. There is only one valine, Val3, in the N-terminus and two leucines, Leu8 and Leu13. Studies of N-terminal deletion mutants (Forsthoefel *et al.*, 2004) have shown that del6 (an hTS variant with residues 1–6 deleted) is more stable to intracellular degradation than the wild-type enzyme. This is consistent with the hypothesis that the inactive conformer is more rapidly degraded and that the N-terminus shifts the active/inactive equilibrium towards the latter. On the other hand, the first residue of the N-terminus that is not disordered, Pro26, is on the other side of the molecule (for both subunits), while the disordered loop 108–129 is in the vicinity. This loop includes Leu118 and Leu121. Another possibility is that the density is a fragment of a neighboring molecule, which would suggest that the crystal lattice shifts the equilibrium towards the inactive conformer. The closest Pro26 is 31 Å away. The hydrophobic pocket includes Trp182 and Leu187, residues from the loop 181–197, but does not contain phosphate/sulfate-binding sites. Thus, ligands binding in this pocket should stabilize the inactive conformer without interfering with mRNA binding.

The crystal form reported here should enable crystal binding studies of inhibitors stabilizing the inactive conformer of hTS and may provide lead compounds for new chemotherapeutic agents exploiting this novel approach to hTS inhibition. A modeling study suggested that a *t*-butanol molecule may fit well in the 'Val3' binding site and a kinetic study showed that it is an uncompetitive inhibitor of hTS with a K_i of 88.5 m*M* (Lovelace, work to be published). *t*-Butanol, if it indeed binds in the predicted site, would fill only a part of the cavity and appropriate larger molecules should be stronger inhibitors.

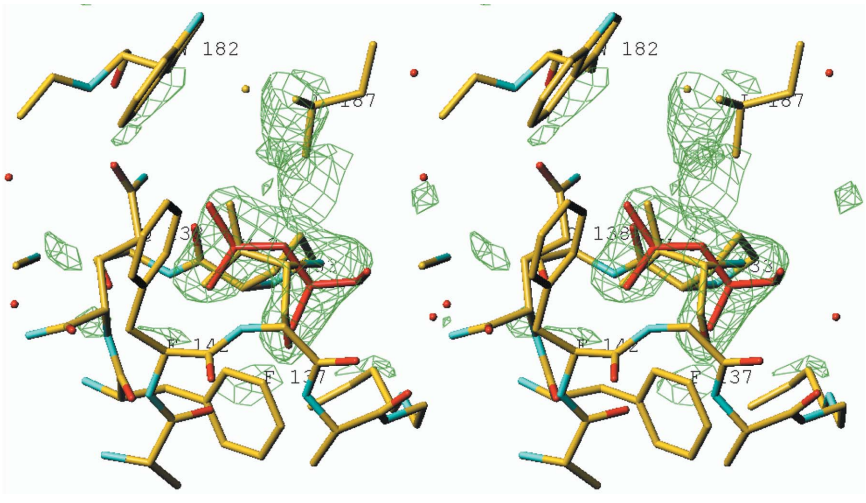

Figure 5
The hydrophobic pocket with a disconnected valine (Val3 in yellow) or leucine (in red) residue. The upper part of the pocket is formed by residues from loop 181–197. In front there is a fragment of density which probably represents another part of the same polypeptide region. This pocket is about 16–18 Å from the sulfate ions and ligand binding in it should stabilize the inactive conformer and should not interfere with mRNA binding.

This work was supported by NIH grant CA076560 and a grant from South Carolina Cancer Center. Use of the Argonne National Laboratory Structural Biology Center beamlines at the Advanced Photon Source was supported by the US Department of Energy, Office of Science under contract W-31-109-ENG-38.

References

Almog, R., Waddling, C. A., Maley, F., Maley, G. F. & Van Roey, P. (2001). *Protein Sci.* **10**, 988–996.

Anderson, A. C., O'Neil, R. H., DeLano, W. L. & Stroud, R. M. (1999). *Biochemistry*, **38**, 13829–13836.

Berger, S. H., Berger, F. G. & Lebioda, L. (2004). *Biochem. Biophys. Acta*, **1696**, 15–22.

Brünger, A. T., Adams, P. D., Clore, G. M., DeLano, W. L., Gros, P., Grosse-Kunstleve, R. W., Jiang, J.-S., Kuszewski, J., Nilges, M., Pannu, N. S., Read, R. J., Rice, L. M., Simonson, T. & Warren, G. L. (1998). *Acta Cryst.* D**54**, 905–921.

Carreras, C. W. & Santi, D. V. (1995). *Annu. Rev. Biochem.* **64**, 721–762.

Chu, E. & Allegra, C. J. (1996). *Bioessays*, **18**, 191–198.

Collaborative Computational Project, Number 4 (1994). *Acta Cryst.* D**50**, 760–763.

Danenberg, K. D. & Danenberg, P. V. (1979). *J. Biol. Chem.* **254**, 4345–4348.

Finer-Moore, J. S., Santi, D. V. & Stroud, R. M. (2003). *Biochemistry*, **42**, 248–256.

Forsthoefel, A. M., Pena, M. M. O., Xing, Y. Y., Rafique, Z. & Berger, F. G. (2004). *Biochemistry*, **43**, 1972–1979.

Houghton, P. J. (1999). *Antifolate Drugs in Cancer Therapy*, edited by A. L. Jackman, pp. 423–436. Totowa, NJ, USA: Humana Press.

Humphries, G. K. & Greenberg, D. M. (1958). *Arch. Biochem. Biophys.* **78**, 275–287.

Kitchens, M. E., Forsthoefel, A. M., Rafique, Z., Spencer, H. T. & Berger, F. G. (1999). *J. Biol. Chem.* **274**, 12544–12547.

Kraulis, P. J. (1991). *J. Appl. Cryst.* **24**, 946–950.

Laskowski, R. A., MacArthur, M. W., Moss, D. S. & Thornton, J. M. (1993). *J. Appl. Cryst.* **26**, 283–291.

Merritt, E. A. & Bacon, D. J. (1997). *Methods Enzymol.* **277**, 505–524.

Nicholls, A., Sharp, K. & Honig, B. (1991). *Proteins Struct. Funct. Genet.* **11**, 281–296.

Otwinowski, Z. & Minor, W. (1997). *Methods Enzymol.* **276**, 307–326.

Phan, J., Koli, S., Minor, W., Dunlap, R. B., Berger, S. H. & Lebioda, L. (2001). *Biochemistry*, **40**, 1897–1902.

Phan, J., Steadman, D. J., Koli, S., Ding, W. C., Minor, W., Dunlap, R. B., Berger, S. H. & Lebioda, L. (2001). *J. Biol. Chem.* **276**, 14170–14177.

Rocchia, W., Alexov, E. & Honig, B. (2001). *J. Phys. Chem. B*, **105**, 6507–6514.

Rocchia, W., Sridharan, S., Nicholls, A., Alexov, E., Chiabrera, A. & Honig, B. (2002) *J. Comput. Chem.* **23**, 128–137.

Roussel, A. & Cambillau, C. (1991). *Silicon Graphics Geometry Partners Directory*, p. 86. Mountain View, CA, USA: Silicon Graphics.

Schiffer, C. A., Clifton, I. J., Davisson, V. J., Santi, D. V. & Stroud, R. M. (1995). *Biochemistry*, **34**, 16279–16287.

Stroud, R. M. & Finer-Moore, J. S. (2003). *Biochemistry*, **42**, 239–247.